RSC Advances

ROYAL SOCIETY OF CHEMISTRY

PAPER

View Article Online
View Journal | View Issue

Check for updates

Cite this: *RSC Adv.*, 2021, **11**, 15351

# Performance of gamma-$Al_2O_3$ decorated with potassium salts in the removal of $CS_2$ from $C_5$ cracked distillate

Xiance Zhang,[a] Guanglin Zhou,*[a] Mengying Wang,[b] Xiaosheng Wang,[a] Weili Jiang[a] and Hongjun Zhou[a]

Received 8th March 2021
Accepted 10th April 2021

DOI: 10.1039/d1ra01819a

rsc.li/rsc-advances

Deep desulfurization is a key process for the production of high value-added products from $C_5$ distillates. In this work, different potassium salt modified gamma-$Al_2O_3$ adsorbents were prepared by an incipient-wetness impregnation method and characterized by $N_2$ adsorption–desorption, SEM-EDS, TEM, $CO_2$-TPD, XRD, FT-IR, and IC. The $C_5$ distillate with a 1200 μg $mL^{-1}$ sulfur content is desulfurized to less than 10 μg $mL^{-1}$ within 24 hours by the static adsorption method. For the desulfurization in the fix-bed reactor, the breakthrough sulfur capacity of $K_2CO_3$-decorated gamma-$Al_2O_3$ reaches 0.76 wt% under the optimized conditions, *viz.*, at 30 °C, with a sulfur content of 50 μg $mL^{-1}$ in the raw oil, and a liquid hourly space velocity of 1 $h^{-1}$. The desulfurization activity of the exhausted adsorbent can be recovered after regeneration. Selective adsorption of $CS_2$ includes three processes: adsorption, hydrolysis, and oxidation. $CS_2$ is first adsorbed on the adsorbent and hydrolyzed to form $H_2S$. $H_2S$ is further oxidized to form $S/SO_4^{2-}$, and then deposits on the surface of the adsorbent. Adsorption, hydrolysis, and oxidation all play essential roles in the removal process of $CS_2$.

## 1 Introduction

$C_5$ distillate is one of the by-products of high-temperature cracking of naphtha to ethylene.[1] Its yield is generally about 14–20% that of ethylene. $C_5$ contains nearly 20 kinds of compounds, including isoprene, cyclopentadiene, and piperylene.[2] Their unique molecular structures can be used to synthesize other chemical products, which have high economic value.[3] In the petrochemical industry, two technologies are commonly used to treat the $C_5$: one method is to separate it into monomers; another way is to use it as a raw material for producing low-carbon olefins after hydrogenation.

The sulfur composition of $C_5$ is different compared with other distillates. When naphtha is cracked to ethylene, it is easy to coke due to the high temperature during the pyrolysis process, which affects the product quality. Salari *et al.*[4] found that different types of sulfides have different effects on coking performance. At a certain sulfur content, the coking rate is as follows: dimethyl disulfide (DMDS) < disulfide oil < dimethyl sulfide < $CS_2$. To reduce the amount of coke and prolong the cracking furnace operating cycle, DMDS and $CS_2$ are selected as coking inhibitors to reduce the coking rate in the industrial production process. Therefore, the main sulfide in the $C_5$ is $CS_2$, with a small number of other sulfides such as thioether, mercaptan, and thiophene. The existence of sulfur compounds greatly impacts the physical properties of catalysts, additives, and products, as well as the processing stability and the value of the products. Although the sulfur content of $C_5$ varies (often in the range of 40–100 μg $mL^{-1}$) from different manufacturers, the main sulfide is always $CS_2$.

In traditional desulfurization technology, the more mature hydrodesulfurization technology results in unnecessary olefin saturation, excessive sulfur species,[5] which is not suitable for the $C_5$. Compared with traditional hydrogen desulfurization, adsorption desulfurization has the advantages of a short process, low energy consumption, and no hydrogen required.[6–8] However, the $C_5$ adsorption desulfurization has not achieved large-scale industrialization due to the insufficient experimental data and unclear desulfurization mechanism. Patent CN101450303A[9] reported a method of adsorbents preparation, they mixed group 8 and group 11 metal salts with sodium hydroxide as the precipitant in an aprotic solvent, then mixed with the $Al_2O_3$ dry glue to obtain the adsorbent. Under certain conditions, the adsorbent could remove almost all sulfide in $C_5$ conjugated diene raw materials. However, this desulfurization process requires hydrogen and a higher operating temperature, which leads to the saturation and polymerization of $C_5$ olefin. Patent CN103182291A[10] used the pseudo-boehmite powder to prepare gamma-$Al_2O_3$ support and then impregnated a mixed solution of $Zn^{2+}$, $Cu^{2+}$, group 1, or group 2 metal to obtain a desulfurization adsorbent. The desulfurization of the cracked $C_5$ using a fixed bed can reduce the sulfur content to 1 μg $g^{-1}$ or lower. However, the adsorbent sulfur capacity is low, and regeneration is difficult.

---

[a] College of New Energy and Materials, China University of Petroleum-Beijing, Beijing, 102249, China. E-mail: zhouguanglin2@163.com

[b] College of Chemical Engineering and Environment, China University of Petroleum-Beijing, Beijing, 102249, China

The methane reaction with sulfur and hydrogen sulfide is considered the leading cause of undesirable $CS_2$ in the modified Claus process.[11] A highly efficient hydrolysis catalyst is required to remove $CS_2$ and COS. The reactions of $CS_2$ hydrolysis are as follows:[12] $CS_2 + H_2O \rightarrow COS + H_2S$, $COS + H_2O \rightarrow CO_2 + H_2S$, $CS_2 + 2H_2O \rightarrow CO_2 + 2H_2S$. The $C_5$ contains a trace amount of water, and the hydrolysis reaction of $CS_2$ may occur. Therefore, using a hydrolysis catalyst to remove $CS_2$ from the $C_5$ would be an effective method.[13,14] In this paper, the gamma-$Al_2O_3$ support is loaded with different potassium salts by an incipient-wetness impregnation method. The $C_5$ distillate is used as raw material. Static adsorption experiments and fixed bed dynamic experiments are carried out to study the adsorption performance of the modified adsorbent on $CS_2$. Furthermore, the desulfurization mechanism is investigated by $N_2$ adsorption–desorption, SEM-EDS, TEM, XRD, $CO_2$-TPD, FT-IR, and IC.

## 2 Results and discussion

### 2.1 Performance of catalysts in static experiments

Fig. 1 shows the desulfurization performance of gamma-$Al_2O_3$ adsorbents decorated by three different potassium salt solutions. The $Al_2O_3$ can remove the $CS_2$ in $C_5$, and the sulfur content in $C_5$ is 989 μg mL$^{-1}$ after 3 hours. After the calcination at 500 °C, the $KNO_3$ in the $KNO_3/Al_2O_3$ catalyst decomposes into $K_2O$ and form an Al–O–K structure with $Al_2O_3$.[15] However, the adsorption desulfurization ability of $KNO_3/Al_2O_3$ is slightly improved, only 16 μg mL$^{-1}$ higher after 3 hours. The $KOH/Al_2O_3$ and $K_2CO_3/Al_2O_3$ improve the adsorption and desulfurization ability of the $Al_2O_3$ support significantly, indicating that the alkaline has good selective adsorption for $CS_2$. The modified $Al_2O_3$ is more alkaline than $Al_2O_3$, which corresponds to the subsequent $CO_2$-TPD characterization. The desulfurization effect of $K_2CO_3/Al_2O_3$ is better than that of $KOH/Al_2O_3$. When the adsorption time is 3 hours, the sulfur content in the product is 412 μg mL$^{-1}$ and 496 μg mL$^{-1}$, respectively. The cause of this phenomenon is analyzed in the next section.

Fig. 2 shows the effect of adsorbents prepared by different concentrations of $K_2CO_3$ on the removal performance of $CS_2$. The desulfurization capacity gradually increases with the increase of $K_2CO_3$ impregnation concentration. When the impregnation concentration of $K_2CO_3$ is 0.3 g mL$^{-1}$, the static desulfurization performance is the greatest, and the sulfur content in $C_5$ can be reduced to less than 10 μg mL$^{-1}$ from 1200 μg mL; however, continue increasing the impregnation concentration $K_2CO_3$ results in decreasing of the desulfurization capacity. This indicates that the amount of alkali has a significant influence on the desulfurization activity. The loading of $K_2CO_3$ affects the alkalinity of the adsorbent surface and the distribution of basic sites in the desulfurizer. The weak base center on the surface of adsorbent is more critical, and the strong alkalinity is not conducive to the adsorption of $CS_2$. Excessive alkalinity causes irreversible adsorption of $CS_2$ and intermediate formation (*i.e.*, $H_2S$ and S) in the adsorbent,[16] covering the active sites, which is why the same loading amount of KOH is not as good as $K_2CO_3$. Consequently, the experimental $K_2CO_3$ immersion concentration is determined as 0.3 g mL$^{-1}$. These results indicate that $OH^-$ on the adsorbent plays a vital role in the adsorption activity.

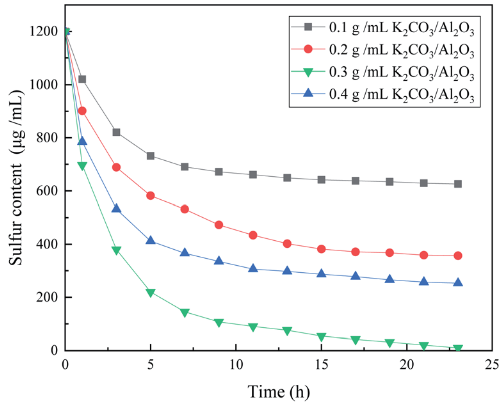

Fig. 2 Removal performance of $CS_2$ over $Al_2O_3$ modified by different $K_2CO_3$ concentration.

The $C_5$ component contains round 80 μg mL$^{-1}$ of water, so we used the 0.3 g mL$^{-1}$ $K_2CO_3/Al_2O_3$ catalyst to investigate the influence of water. In Fig. 3, as the concentration of added water

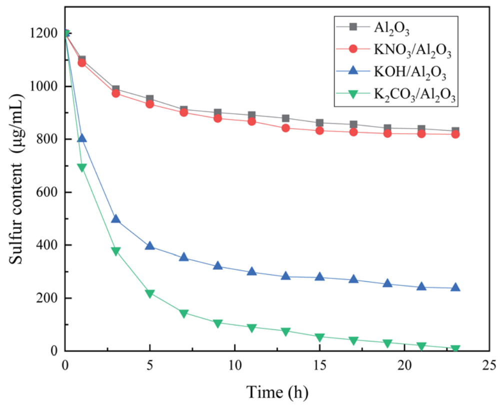

Fig. 1 Removal performance of $CS_2$ over $Al_2O_3$ modified by different precursors.

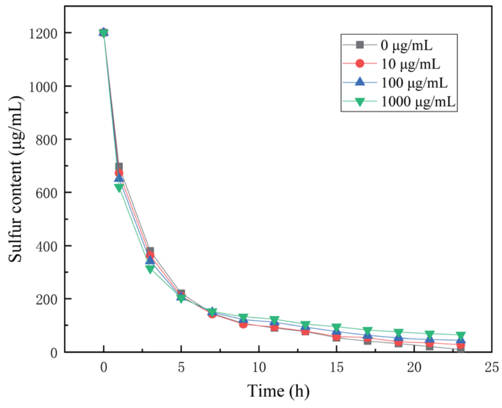

Fig. 3 Effect of water on the removal performance.

increases, the initial desulfurization rate gradually increases, which shows that the addition of water promotes the hydrolysis rate of $CS_2$. However, with the further progress of desulfurization, $CS_2$ the final desulfurization result decreases with added water. The water may compete with $CS_2$ for adsorption, resulting in the weakening of the adsorption capacity of $CS_2$.[17] The increase in water is also beneficial to the oxidation rate. Primavera *et al.*[18] believed that water plays an essential role in the oxidation of $H_2S$. The increase of water content can promote the deposition of sulfur products on the catalyst, resulting in an increasing deactivation rate. As the addition of water increases, the water cannot dissolve thoroughly in the $C_5$, resulting in the separation of oil and water. Therefore, the addition of water cannot improve the performance of the catalyst but reduce the quality of the products.

### 2.2 Performance of catalysts in fixed-bed reactor

In order to investigate the effect of reaction conditions on the adsorption performance of modified $Al_2O_3$, the fixed bed was used to study the dynamic adsorption performance of 0.3 g $mL^{-1}$ $K_2CO_3/Al_2O_3$ catalyst. Fig. 4 shows the effect of (a) sulfur contents, (b) LSHVs, and (c) reaction temperature on the adsorption desulfurization performance in the dynamic desulfurization process of $C_5$ distillate.

Sulfur content is one of the most important factors affecting the desulfurization capacity of the adsorbent. When the raw material sulfur content is 50, 75, and 100 μg $mL^{-1}$, the breakthrough sulfur capacity is 0.76 wt%, 0.60 wt%, and 0.46 wt%, respectively. The increase in the sulfur content of $C_5$ means that $H_2S$ generation increases, which also causes an increase in oxidation products of S and sulfate. The corresponding sulfur products deposit on the surface of the adsorbent, cover the active sites, and hinder the conversion of $CS_2$. Therefore, the increase of sulfur content in $C_5$ leads to the decrease of the adsorption desulfurization performance of the adsorbent.

The prepared $K_2CO_3/Al_2O_3$ adsorbent is used to investigate the effect of different LHSVs on the desulfurization performance of the adsorbents at room temperature. Fig. 4(b) shows that the adsorption capacity of the adsorbent for $CS_2$ gradually decreases as the space velocity increases. When the space velocity is 0.5, 1.0, and 1.5 $h^{-1}$, the breakthrough sulfur content is 0.86 wt%, 0.76 wt%, and 0.50 wt%, respectively. When the feedstock feed amount is low, the $CS_2$ molecule in the $C_5$ oil has a longer residence time on the surface of the adsorbent, which can promote its adsorption and diffusion process. So, the adsorption performance is better at low space velocity. However, when the space velocity is 0.5 $h^{-1}$, the amount of raw material oil processed per unit time is too small to meet industrial demand. When the space velocity is too high, the contact time between $CS_2$ and the surface of the adsorbent is shortened, which is not conducive to the adsorption desulfurization process of the adsorbent. Therefore, it is most suitable for industrial applications when the space velocity is 1.0 $h^{-1}$.

The prepared 0.3 g $mL^{-1}$ $K_2CO_3/Al_2O_3$ adsorbent is applied to examine the effect of different adsorption temperatures on the desulfurization performance of the adsorbent at an adsorption LSHV of 1.0 $h^{-1}$. The influence of temperature on the desulfurization effect is shown in Fig. 4(c). This experiment selects a temperature range of 5–55 °C. At 5 °C, the breakthrough sulfur capacity is 0.57 wt%. It is because the hydrolysis reaction rate of $CS_2$ in $C_5$ is low at a relatively lower temperature, resulting in poor desulfurization activity of the adsorbent. With the increase of temperature, the hydrolysis rate increases, and the reaction is more likely to occur. Besides, high temperature also favors the oxidation of $H_2S$, facilitating the next reaction.

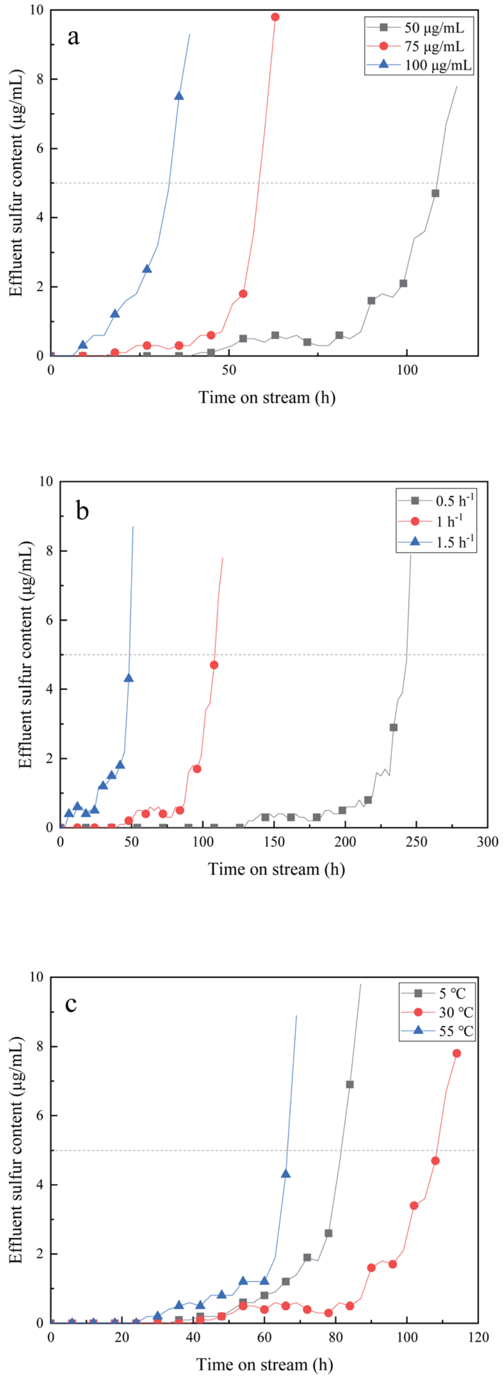

Fig. 4 Effect of (a) sulfur content of raw materials, (b) LHSV, and (c) temperature on removal performance of $CS_2$.

When the temperature is 30 °C, the breakthrough sulfur capacity is 0.76 wt%, and the desulfurization effect is best. The increase in the temperature leads to a gradual rise of $SO_4^{2-}$/S ratio.[19] Sulfate is formed more rapidly, causing catalyst poisoning and inhibiting the progress of the hydrolysis reaction. When the temperature is 55 °C, the breakthrough sulfur capacity of the adsorbent is 0.47 wt%, which is not suitable for the desulfurization of $C_5$. Besides, the product begins to turn yellow at 55 °C, indicating that the product has been aggregated, thus affecting desulfurization activity and product quality.

### 2.3 Evaluation of regeneration performance of adsorbents

The performance evaluation of regenerated adsorbents is carried out in a fixed bed reactor, and its results are shown in Table 1. The evaluation conditions are 30 °C, with a sulfur content of 50 μg mL$^{-1}$ in the raw oil, and an LHSV of 1 h$^{-1}$. The sulfur capacity of the adsorbent is 0.74 wt% for the first regeneration and 0.71 wt% for the second regeneration. The adsorbent shows good regeneration performance.

### 2.4 Characterization of the adsorbents

Table 2 shows the pore structure parameters of the adsorbents prepared *via* different concentrations of $K_2CO_3$. It can be seen from Table 2 that as the $K_2CO_3$ loading increases, the average pore size increases slightly, while the specific surface area and total pore volume decrease significantly. After loading $K_2CO_3$, the average pore size increase is due to the pores being filled with $K_2CO_3$, rather than the pore size becoming larger due to impregnation. The decrease in specific surface area and total pore volume is due to the filling of $K_2CO_3$, the small pore size disappears, and the large pore size becomes small. When the loading of $K_2CO_3$ increases from 0.3 g mL$^{-1}$ to 0.4 g mL$^{-1}$, a large amount of $K_2CO_3$ is deposited on the surface, the specific surface area decreased from 211.79 m$^2$ g$^{-1}$ to 158.54 m$^2$ g$^{-1}$, and the total pore volume decreased from 0.37 cm$^3$ g$^{-1}$ to 0.31 cm$^3$ g$^{-1}$.

Fig. 5(a) is an isotherm adsorption–desorption curve of different concentrations of $K_2CO_3/Al_2O_3$ adsorbent. In Fig. 5, the isothermal adsorption–desorption curves of different $K_2CO_3/Al_2O_3$ adsorbents are type IV and have the same H hysteresis loop in medium pressure and high-pressure parts ($0.4 < P/P_0 < 1$), which is generally considered to be interconnected by the pore size of the mesoporous material.[20] In the low-pressure section, the adsorption amount is gently increased, and $N_2$ molecules are adsorbed on the mesopores inner surface in a single layer to a plurality of layers. There is a sudden increase in the adsorption amount at $P/P_0 = 0.4–0.8$, which means that the mesoporous structure is relatively uniform. The pore size distribution of the adsorbent is obtained by the Barrett–Joyner–Halenda method (BJH), which is shown in Fig. 5(b). Interaction between the $K_2CO_3$ with the support $Al_2O_3$ does not significantly change the structure.[21] The pore size distribution of the adsorbent loaded with different concentrations of $K_2CO_3$ is similar, mainly concentrated at 4–5 nm. When the $K_2CO_3$ loading is 0.3 g mL$^{-1}$, the pore diameter is the smallest, which is mainly about 4.3 nm. The pore size of this range is suitable for the adsorption of $CS_2$, and the adsorption desulfurization performance is best.

Fig. 6 shows the SEM image of virgin $Al_2O_3$, fresh 0.2 g mL$^{-1}$, 0.3 g mL$^{-1}$, 0.4 g mL$^{-1}$ $K_2CO_3/Al_2O_3$ adsorbent and deactivated 0.3 g mL$^{-1}$ $K_2CO_3/Al_2O_3$ adsorbent. When $K_2CO_3$ is not loaded, the surface of $Al_2O_3$ is very rough with a large number of holes, which is an irregular block structure. After the loading of $K_2CO_3$, the pores of $Al_2O_3$ are filled with $K_2CO_3$, and the surface becomes smooth gradually. The unfilled $K_2CO_3$ is loaded on the surface of the support in the form of small particles. As the

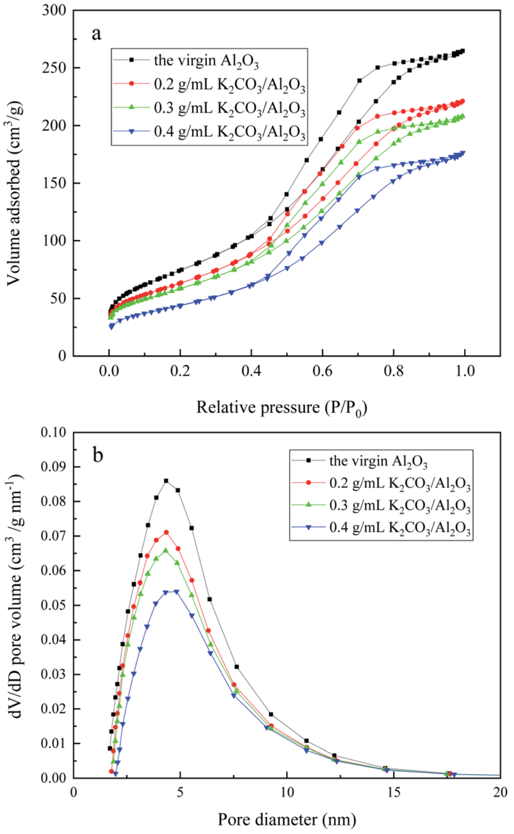

Fig. 5 (a) Adsorption isotherm and (b) PSD of gamma-$Al_2O_3$ and supported $K_2CO_3$ based adsorbents.

Table 1 Breakthrough sulfur capacity of adsorbents with different regeneration times

| Regeneration times | 0 | 1 | 2 |
|---|---|---|---|
| Sulfur capacity (wt%) | 0.76 | 0.74 | 0.71 |

Table 2 Structural characteristics of prepared $K_2CO_3/Al_2O_3$ adsorbents

| $K_2CO_3$ concentration (g mL$^{-1}$) | 0.0 | 0.2 | 0.3 | 0.4 |
|---|---|---|---|---|
| BET surface area (m$^2$ g$^{-1}$) | 272.09 | 229.27 | 211.79 | 158.54 |
| Total pore volume (cm$^3$ g$^{-1}$) | 0.47 | 0.39 | 0.37 | 0.31 |
| Average pore diameter (nm) | 6.02 | 6.07 | 6.08 | 6.89 |

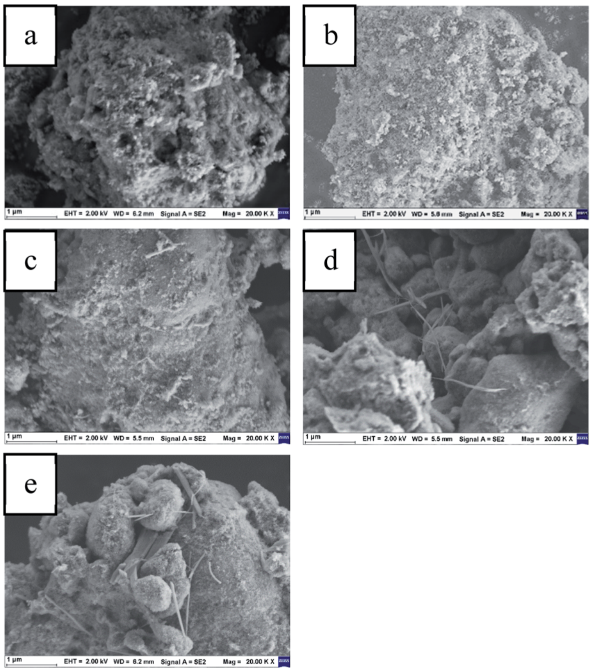

Fig. 6 SEM of (a) the virgin-$Al_2O_3$, (b–d) the fresh 0.2 g mL$^{-1}$, 0.3 g mL$^{-1}$, 0.4 g mL$^{-1}$ $K_2CO_3/Al_2O_3$, (e) the exhausted 0.3 g mL$^{-1}$ $K_2CO_3/Al_2O_3$.

loading increased, filamentous $K_2CO_3$ crystals appeared on the surface of the 0.4 g mL$^{-1}$ $K_2CO_3/Al_2O_3$ adsorbent.

When 0.3 g mL$^{-1}$ $K_2CO_3/Al_2O_3$ adsorbent adsorbs $CS_2$, the product produced by the adsorption process will block the pores and accumulate on the surface, one of the reasons for the decreased activity after adsorption of $CS_2$.[22] Among them, many kinds of filamentous or banded crystals appear on the surface of the adsorbed $Al_2O_3$ support. Since the loading of K did not increase, the crystals that appeared are associated with the adsorbed products, and the specific results are further analyzed by TEM.

Table 3 shows the EDS characterization result corresponding to the SEM. Virgin-$Al_2O_3$ contains only Al and O elements, and other elements are almost zero. After loading $K_2CO_3$, the content of the K element gradually increases as the amount of load increases. When the load concentration of $K_2CO_3$ is increased from 0.3 g mL$^{-1}$ to 0.4 g mL$^{-1}$, the mass increase of K is small, probably because the pores are already filled with $K_2CO_3$, and excessive K species blocks the pores and enriches the surface, resulting in a decrease in the loading mass. When $CS_2$ is adsorbed, the presence of the S element can be detected, and the mass is 1.23 wt%, which means that the S element can be well adsorbed on the $K_2CO_3/Al_2O_3$ adsorbent.

Table 3 EDS analysis of the surface of fresh and exhausted $K_2CO_3/Al_2O_3$

| | | Al | O | K | S |
|---|---|---|---|---|---|
| Virgin $Al_2O_3$ | at.% | 39.62 | 60.28 | 0.10 | 0.01 |
| | wt% | 47.33 | 52.47 | 0.19 | 0.01 |
| Fresh 0.2 g mL$^{-1}$ $K_2CO_3/Al_2O_3$ | at.% | 36.18 | 60.25 | 3.52 | 0.05 |
| | wt% | 46.95 | 46.35 | 6.62 | 0.07 |
| Fresh 0.3 g mL$^{-1}$ $K_2CO_3/Al_2O_3$ | at.% | 29.68 | 62.54 | 7.74 | 0.03 |
| | wt% | 38.04 | 47.52 | 14.38 | 0.05 |
| Fresh 0.4 g mL$^{-1}$ $K_2CO_3/Al_2O_3$ | at.% | 30.47 | 60.24 | 9.28 | 0.01 |
| | wt% | 38.25 | 44.85 | 16.89 | 0.01 |
| Exhausted 0.3 g mL$^{-1}$ $K_2CO_3/Al_2O_3$ | at.% | 32.34 | 61.25 | 5.61 | 0.80 |
| | wt% | 41.60 | 46.72 | 10.46 | 1.23 |

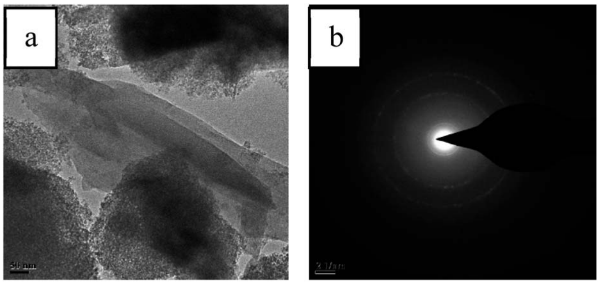

Fig. 7 (a) TEM images of exhausted 0.3 g mL$^{-1}$ $K_2CO_3/Al_2O_3$ adsorbent and (b) diffraction pattern taken from region c marked in (a).

Since a newly formed crystal are found in the SEM image after desulfurization, TEM analysis is used. Fig. 7 shows a TEM image of the 0.3 g mL$^{-1}$ $K_2CO_3/Al_2O_3$ adsorbent adsorbed by $CS_2$ and a diffraction pattern of the adsorbed product. After the adsorption of $CS_2$, a wafer appears around the adsorbent, and three crystal rings appear in the diffraction pattern, which is analyzed and calculated. Comparing the calculated Di with the PDF card, it is found that the three Di are 5.756, 1.988, and 1.374, respectively, corresponding to the three diffractive crystal surface (113), (408), and (288) of the S element, which conforms to the S elemental crystal (JCPDS No. 83-2283), demonstrating the formation of elemental S in the products.

Fig. 8 is the $CO_2$-TPD spectra of the 0.3 g mL$^{-1}$ $KNO_3/Al_2O_3$, $K_2CO_3/Al_2O_3$, and $KOH/Al_2O_3$ adsorbents. For both $K_2CO_3/Al_2O_3$ and $KOH/Al_2O_3$ adsorbents, there are two $CO_2$ desorption peaks at a lower temperature (~100 °C) and higher temperature (~600 °C), which belong to the weak base and strong base centers, respectively. Besides, both peak strength and temperature of

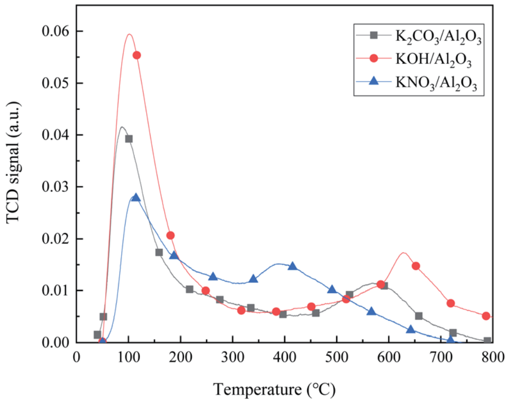

Fig. 8 $CO_2$-TPD spectra of 0.3 g mL$^{-1}$ $KNO_3/Al_2O_3$, $K_2CO_3/Al_2O_3$, and $KOH/Al_2O_3$ adsorbents.

KOH adsorbent are higher than those of $K_2CO_3$, indicating that the alkalinity of $KOH/Al_2O_3$ is stronger than that of $K_2CO_3/Al_2O_3$ adsorbent. $KNO_3/Al_2O_3$ adsorbent has only one weak base and one medium strong base adsorption center, and the desulfurization effect is only improved a little compared with pure $Al_2O_3$ adsorbent. In the desulfurization process, the hydrolysis center is $OH^-$, and water plays a role in supplementing $OH^-$.[23,24] However, high alkalinity is not favorable for the hydrolysis of $CS_2$ because $CS_2$ and its final hydrolyzed products ($H_2S$ and $CO_2$) are easily irreversibly adsorbed on the surface,[16] inhibiting the catalytic hydrolysis reaction. Therefore, the adsorption and hydrolysis capacity of KOH with strong alkalinity is weaker than that of $K_2CO_3$.

Fig. 9 is an XRD spectrum of $K_2CO_3$, $Al_2O_3$ support, fresh 0.3 g $mL^{-1}$ $K_2CO_3/Al_2O_3$ adsorbent, and exhausted 0.3 g $mL^{-1}$ $K_2CO_3/Al_2O_3$ adsorbent. The main peaks of pure $K_2CO_3$ XRD images are at $2\theta = 26.3$, 30.1, 32.2, 34.3, and 42.9°, which are consistent with PDF cards (JCPDS No. 71-1466).[25] The peaks of the XRD images of the support are mainly at $2\theta = 19.5$, 37.6, 39.4, 45.8, 60.8, and 67.0°, which is consistent with the position of the main peak of gamma-$Al_2O_3$ (JCPDS No. 10-0425). Compared with gamma-$Al_2O_3$, the strength of the main peak after $K_2CO_3$ modification is lower, and a new $K_2CO_3$ peak is generated at $2\theta = 32.2$ and 34.3°. The peak intensity is lower than pure $K_2CO_3$, which means that $K_2CO_3$ has a good load on the $Al_2O_3$ and has good dispersion.[25] Liu *et al.*[26] found that the $K_2CO_3/Al_2O_3$ adsorbent after calcining at 500 °C contained $K_2O$, which may be overlaid in the XRD spectra due to lower content. Therefore, the composition of $K_2CO_3/Al_2O_3$ adsorbent is $K_2CO_3$, $Al_2O_3$, and a small amount of $K_2O$.

When the adsorbent adsorbs $CS_2$, no peak of elemental S was found because the generated elemental S is easily sublimated in the air, resulting in too little amount on the surface of the adsorbent being difficult to detect. At $2\theta = 26.4$ and 29.8°, there is a new peak generation, and the peak intensity at $2\theta = 30.8°$ increases, which is the characteristic peak of $K_2SO_4$ (JCPDS No. 73-1674), which means the production of $SO_4^{2-}$ after adsorption of $CS_2$. The peak intensity of $Al_2O_3$ and $K_2CO_3$ after adsorption is reduced due to the deposition of sulfur products formed by adsorption of $CS_2$ on the adsorbents.

Fig. 10 is a Fourier infrared spectrum of the 0.3 g $mL^{-1}$ $K_2CO_3/Al_2O_3$ adsorbent before and after the adsorption of $CS_2$. It can be seen from Fig. 10 that the peak appearing around 3558 $cm^{-1}$ is a characteristic peak of –OH,[27–29] which is derived from the –OH in $K_2CO_3/Al_2O_3$ adsorbent during catalyst preparation. The peaks at 1400 $cm^{-1}$ and 1580 $cm^{-1}$ are characteristic peaks of –COO and –C=O, which are related to the supported potassium carbonate $CO_2$.[26] –COO and –C=O promote the oxidation of $H_2S$, which accelerates the reaction rate of $H_2S$ by $O_2$ to S, further improving the conversion ability of $CS_2$. The peaks at 787 $cm^{-1}$ ($AlO_4$) and 582 $cm^{-1}$ ($AlO_6$) are related to the Al–O–Al structure.[30]

After adsorption of $CS_2$, new peaks at 2329 $cm^{-1}$ and 2370 $cm^{-1}$ are related to $CO_2$,[31] indicating that the $CO_2$ produced by hydrolysis is chemically adsorbed to the adsorbent. The peaks at 2919 $cm^{-1}$ and 2850 $cm^{-1}$ are related to $-CH_3$ and $-CH_2$, indicating the residual of the adsorbed $C_5$ on the adsorbent. The peaks at 1383 $cm^{-1}$ and 1129 $cm^{-1}$ are related to $SO_4^{2-}$, which means that sulfite or sulfate may form. The peak at 617 $cm^{-1}$ represents the formation of elemental S,[32] and the adsorbed $CS_2$ produces elemental sulfur on the surface of the $K_2CO_3/Al_2CO_3$ adsorbent. This result is consistent with that reported in the literature.[33]

Although we have used XRD and FT-IR to find sulfate group, due to its small content, the peak is not obvious, and it is not

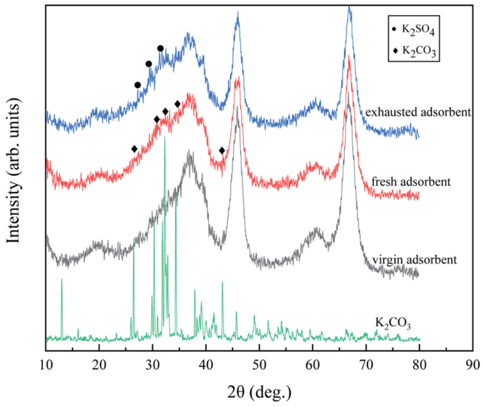

Fig. 9 XRD spectra of the $K_2CO_3$, the virgin adsorbent, the fresh adsorbent, and the exhausted adsorbent.

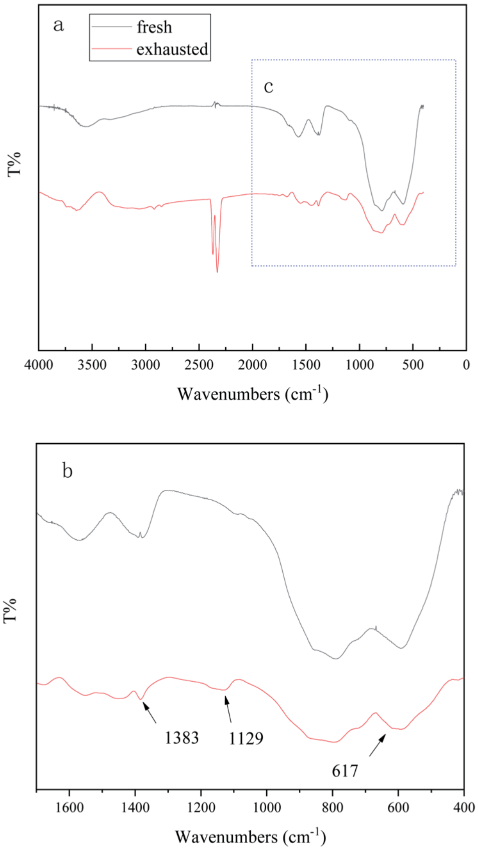

Fig. 10 FT-IR spectra of (a) the fresh and exhausted $K_2CO_3/Al_2O_3$ adsorbents and (b) the enlarged area c marked in (a).

Table 4 Sulfate and sulfite contents of the fresh and the spent catalysts

| | The fresh adsorbent | The spent adsorbent |
|---|---|---|
| $SO_4^{2-}$ (wt%) | 0.00 | 2.62 |
| $SO_3^{2-}$ (wt%) | 0.00 | 0.00 |

possible to distinguish sulfate group from sulfite group. So, the contents of sulfate and sulfite in the fresh and the spent catalysts are analyzed by IC to better explore the sulfur species on the adsorbent. The IC results in Table 4 show that there are no sulfates and sulfites in the fresh adsorbents. The exhausted adsorbent contains 2.62 wt% sulfate but no sulfite. The accumulation of sulfate on the catalyst is the main reason for the decrease of $CS_2$ adsorption performance.

### 2.5 Discussion on the reaction mechanism

When the $K_2CO_3/Al_2O_3$ adsorbent adsorbs $CS_2$ in $C_5$, the adsorbent gradually turns yellow due to the accumulation of sulfur on the adsorbent.[34] After adsorbed $K_2CO_3/Al_2O_3$ is taken out, and it is a yellow granule after grinding. The sulfur smell is dissipated, and the yellow color gradually becomes lighter as time lapses. The adsorbent is further ground to powder. The powder completely turned white after 2 hours, as shown in Fig. 11. This is because $CS_2$ adsorbs on the adsorbent and is converted into elemental S, and elemental S is disappeared when exposed to the air.

The removal process of $CS_2$ in $C_5$ distillate includes three processes of adsorption, hydrolysis, and oxidation. The adsorption is related to the pore structure of $Al_2O_3$ and active components. The $OH^-$ on the support is mainly derived from $K_2CO_3$ which is essential for the $CS_2$ conversion.[35,36] During the hydrolysis process, trace water in the $C_5$ distillate oil and a large number of $OH^-$ on the adsorbent can hydrolyze $CS_2$ to $H_2S$. The $C_5$ contains approximately 50–70 μg $mL^{-1}$ of dissolved $O_2$; the $O_2$ then oxidizes $H_2S$ to elemental S or $SO_4^{2-}$, covering the active site of the adsorbent, resulting in a decrease in adsorption capacity.[37] During this period, $OH^-$, –COO and C═O act to promote oxidation.[38] The specific process is shown in Fig. 12.

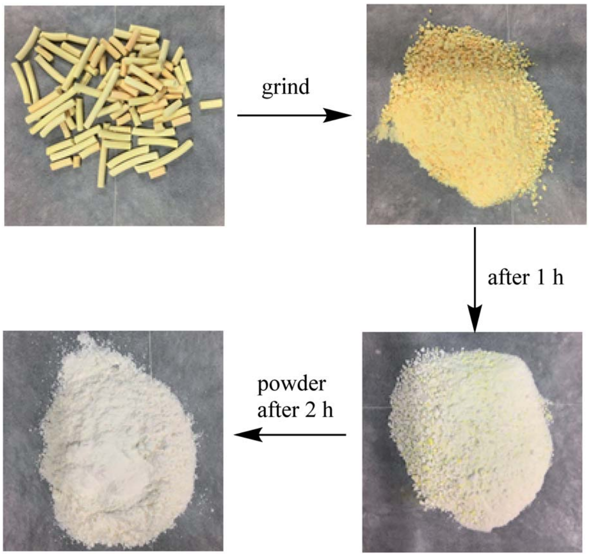

Fig. 11 The macro morphology of exhausted adsorbent.

## 3 Methods

### 3.1 Materials

The pseudo-boehmite powder and sesbania powder were purchased from Shandong Zibo Hengyi Chemical Technology Co., Ltd. $K_2CO_3$ was purchased from Tianjin Reagent Factory no. 3 Factory (A. R.), and potassium nitrate was purchased from Beijing Chemical Plant (A. R.).

### 3.2 Preparation of adsorbent

A certain amount of pseudo-boehmite powder was mixed with an appropriate amount of sesbania powder. 2 wt% dilute nitric acid solution was added to the mixed powder and mixed well. After kneading in a squeezer for 90 min, the template was extruded and dried at 120 °C for 12 h followed by calcination in air at 500 °C for 4 hours to prepare strip-shaped gamma-$Al_2O_3$ support.

The same concentration (0.3 g $mL^{-1}$) of $KNO_3$, KOH, $K_2CO_3$ solution and different concentrations (0.1 g $mL^{-1}$, 0.2 g $mL^{-1}$, 0.3 g $mL^{-1}$, and 0.4 g $mL^{-1}$) of $K_2CO_3$ solution were prepared. The gamma-$Al_2O_3$ support was impregnated with these solutions, respectively, by an incipient-wetness impregnation method, dried at 120 °C for 12 hours, and then calcined at 500 °C for 4 hours to obtain the corresponding potassium salt modified gamma-$Al_2O_3$ desulfurization adsorbents. They were denoted as 0.3 g $mL^{-1}$ $KNO_3/Al_2O_3$, 0.3 g $mL^{-1}$ $KOH/Al_2O_3$, 0.1 g $mL^{-1}$ $K_2CO_3/Al_2O_3$, 0.2 g $mL^{-1}$ $K_2CO_3/Al_2O_3$, 0.3 g $mL^{-1}$ $K_2CO_3/Al_2O_3$, and 0.4 g $mL^{-1}$ $K_2CO_3/Al_2O_3$. Before the experiments, the catalyst was calcined at 400 °C to remove the $H_2O$ and $CO_2$.

The regeneration performance of adsorbents was also investigated. The deactivated adsorbents were calcined at 500 °C in the air atmosphere for 3 hours and then cleaned with deionized water for 3 times to remove the deposited sulfate.

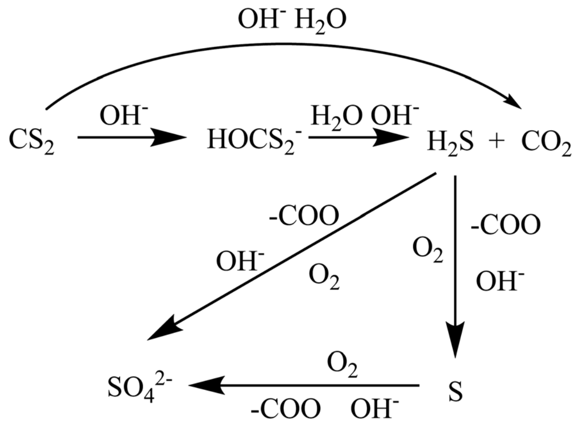

Fig. 12 The mechanism of removal of $CS_2$ by $K_2CO_3/Al_2O_3$.

After that, 0.1 g mL$^{-1}$ $K_2CO_3$ solution was used for reimpregnation to obtain the regenerated adsorbent.

### 3.3 Desulfurization performance tests

The cracked $C_5$ distillate was used as raw material, and 0.12 g and 0.005 g of $CS_2$ was added to 100 mL of cracked $C_5$ distillate, respectively. The mixture was stirred until $CS_2$ was completely dissolved. The sulfur contents in the as-prepared $C_5$ oil were 1200 μg mL$^{-1}$ and 50 μg mL$^{-1}$, respectively. 0.001 g, 0.01 g, and 0.1 g of water were added to 100 mL of prepared $C_5$ distillate, respectively. The final water content of the $C_5$ oil is 10 μg mL$^{-1}$, 100 μg mL$^{-1}$, and 1000 μg mL$^{-1}$, respectively.

The static adsorption method was applied to investigate the adsorption performance of $CS_2$. The experimental conditions were as follows: the adsorption temperature was 30 °C, and 5 g of the modified desulfurization adsorbent was added to 50 mL of $C_5$. The adsorption performance is determined by evaluating the sulfur content of the $C_5$ distillate after adsorption.

The dynamic desulfurization experiment was carried out in a fixed bed reactor at a pressure of 0.4 MPa. The volume of the reaction tube was 30 mL. The sulfur-containing $C_5$ distillate oil is passed through a micro-injection pump from the bottom to the top through a fixed bed with 21 g of modified adsorbent. The effects of temperatures (5, 30 and, 55 °C), different sulfur contents of raw material (50, 75, and 100 μg mL$^{-1}$), and different liquid hourly space velocities (LHSV) (0.5, 1.0, and 1.5 h$^{-1}$) on desulfurization performance of the adsorbent were investigated. During the experiment, $C_5$ was collected at the fixed bed outlet at intervals, and the sulfur content was analyzed. When the sulfur content of the $C_5$ was higher than 5 μg mL$^{-1}$, it was considered that the adsorbent was exhausted, and the experiment was stopped. The calculation formula of the adsorbent breakthrough sulfur capacity $S_C$ (wt%) is shown in eqn (1),

$$\mathrm{S_C} = \frac{V(S_{\mathrm{in}} - S_{\mathrm{out}}) \times t \times 10^{-6}}{m} \times 100 \tag{1}$$

where $V$ is the inlet flow rate (mL h$^{-1}$) of $C_5$ distillate, $S_{\mathrm{in}}$ and $S_{\mathrm{out}}$ are the sulfur content (μg mL$^{-1}$) of $C_5$ at the inlet and outlet of the reaction tube, respectively. And $t$ is the breakthrough time (h), and $m$ is the mass of the adsorbent (g).

Total sulfur content in the liquid of $C_5$ before and after the reaction was analyzed using an RPP-2000S UV fluorescence sulfur analyzer.

### 3.4 Characterization of catalysts

The Brunauer–Emmett–Teller (BET) surface area and total pore volume of the adsorbent were measured using an $N_2$ adsorption–desorption apparatus (TriStar II 3020). The total pore volume was calculated by the amount of $N_2$ adsorbed at a relative pressure ($P/P_0$) = 0.99. The total area was calculated using a multipoint BET surface area calculation method. The morphology of the surface of the adsorbent particles was observed by a field emission scanning electron microscope (SEM, Zeiss Sigma 500). The surface elemental analysis of the adsorbents was measured by an energy spectrometer (EDS, Bruker XFlash 6/30). Transmission electron microscopy image (TEM) was measured using F-20 microscopy (FEI, USA). $CO_2$-TPD was characterized using a Micro Chemitics Instrument's Auto Chem II Model 2920 Multi-Function Adsorber. The catalyst was first purged in helium at a temperature of 400 °C for 1 h, cooled to room temperature, and saturated with pure $CO_2$ at a flow rate of 50 mL min$^{-1}$ for 30 min. After that, the TPD experiment was started, the heating rate was 10 °C min$^{-1}$, the helium flow rate was 50 mL min$^{-1}$, and the temperature was raised to 800 °C. XRD was characterized by a Panaco Sharp Xpert Pro MPD instrument for fresh $K_2CO_3/Al_2O_3$ adsorbents and exhausted adsorbents. The test conditions were: Cu Kα ray, voltage 36 kV, current 30 mA, scanning range 10–80°, step size 0.02° s$^{-1}$. The FT-IR was tested using a Nicoleti S50 infrared spectrometer from PerkinElmer. The sample was mixed and milled with KBr before testing, and the infrared wavelength ranged from 4000 to 400 cm$^{-1}$. Ionic chromatography (IC) was tested by Thermo Dionex ICS-1100. Samples were prepared using 0.10 N NaOH to extract sulfate and sulfite from the spent catalysts using sonication.

## 4 Conclusions

In this paper, we prepared $K_2CO_3/Al_2O_3$ adsorbents to remove $CS_2$ from $C_5$ distillate. When the $K_2CO_3$ loading concentration is 0.3 g mL$^{-1}$, the desulfurization capacity is the best, and the $C_5$ fraction oil with a sulfur content of 1200 μg mL$^{-1}$ can be desulfurized to below 10 μg mL$^{-1}$. The use of the adsorbent in a fixed bed reactor also exhibits good adsorptive desulfurization capabilities. When the sulfur content is 50 μg mL$^{-1}$, the space velocity is 1 h$^{-1}$, and the temperature is 30 °C, the sulfur content can be reduced to 5 μg mL$^{-1}$ or less and maintained for 108 hours. Under the optimized operating conditions, the breakthrough sulfur capacity is 0.76 wt%. The second and third regeneration capacities of the adsorbent were 74 wt% and 71 wt%, respectively. Based on the evidence of surface chemical characterization data, the removal mechanism of $CS_2$ is proposed. The process of desulfurization of $C_5$ distillate oil includes adsorption, hydrolysis, and oxidation. The adsorption is related to the pore structure of the adsorbents and the active components. The hydrolysis and oxidation processes are consistent with the removal of $CS_2$ in the Claus plant. Further work would be to explore the regeneration mechanism of the deactivated adsorbent.

## Author contributions

Xiance Zhang: methodology, investigation, formal analysis, data curation, writing-original draft, Guanglin Zhou: conceptualization, writing-review & editing, project administration, resources, supervision, Mengying Wang: formal analysis, writing-review & editing, Xiaosheng Wang: writing-review & editing, resources, Weili Jiang: writing-review & editing, Hongjun Zhou: supervision.

## Conflicts of interest

There are no conflicts to declare.

## Acknowledgements

We are grateful to the financial supports from the Science Foundation of the China University of Petroleum, Beijing (No. 2462018YJRC028), China Postdoctoral Science Foundation (2019M660931).

## References

1 J. Y. Hou, F. Guo, Q. Hu, Y. Li and Z. M. Hou, *Chin. J. Polym. Sci.*, 2019, **37**, 674–680.
2 H. C. Hsu, S. J. Wang, J. D. Y. Ou and D. S. H. Wong, *Ind. Eng. Chem. Res.*, 2015, **54**, 9798–9804.
3 H. Miki, *J. Jpn. Pet. Inst.*, 2019, **62**, 245–254.
4 D. Salari, A. Niaei, J. Towfighi and P. Panahi, *Iran. J. Chem. Chem. Eng.*, 2006, **2**, 40–51.
5 S. Brunet, D. Mey, G. Pérot, C. Bouchy and F. Diehl, *Appl. Catal., A*, 2005, **278**, 143–172.
6 W. Jiang, X. Gao, L. Dong, J. Xiao, L. H. Zhu, G. Y. Chen, S. H. Xun, C. Peng, W. S. Zhu and H. M. Li, *Pet. Sci.*, 2020, **17**, 1422–1431.
7 Y. Liu, Y. Pan, H. Wang, Y. Liu and C. Liu, *Chin. J. Catal.*, 2018, **39**, 1543–1551.
8 M. A. Larrubia, A. d. Gutièrrez-Alejandre, J. Ramìrez and G. Busca, *Appl. Catal., A*, 2002, **224**, 167–178.
9 C. Li, Z. Jiang, Y. Zhang, Y. Yang, M. Yang and L. Wang, *Chinese Pat.*, CN101450303A, 2009.
10 H. Yu, J. Nan, J. Zhang, Y. Zhang, X. Qu, S. Geng and Y. Shi, *Chinese Pat.*, CN103182291A, 2013.
11 K. Karan and L. A. Behie, *Ind. Eng. Chem. Res.*, 2004, **43**, 3304–3313.
12 C. Deng, X. P. Wu, X. M. Sun, Y. Ren and Y. H. Sheng, *J. Comput. Chem.*, 2009, **30**, 285–294.
13 P. D. Clark, N. I. Dowling and M. Huang, *Appl. Catal., B*, 2001, **31**, 107–112.
14 F. I. Khalili, M. Sultan, C. Robl and M. A. Al-Ghouti, *J. Ind. Eng. Chem.*, 2015, **28**, 282–293.
15 M. Song, X. Yang and G. Wang, *RSC Adv.*, 2018, **8**, 35014–35022.
16 H. Yi, D. He, X. Tang, H. Wang, S. Zhao and K. Li, *Fuel*, 2012, **97**, 337–343.
17 N. Pechler and G. Emig, *Gas Sep. Purif.*, 1991, **5**, 247–251.
18 A. Primavera, A. Trovarelli, P. Andreussi and G. Dolcetti, *Appl. Catal., A*, 1998, **173**, 185–192.
19 L. Wang, D. Wu, S. Wang and Q. Yuan, *J. Environ. Sci.*, 2008, **20**, 436–440.
20 S. Naumov, R. Valiullin and J. Kärger, *Diffus. Fundam.*, 2007, **6**, 67.61–67.62.
21 A. E. Aksoylu, A. N. Akin, S. G. Sunol and Z. İ. Önsan, *Turk. J. Chem.*, 1996, **20**, 88–94.
22 X. Song, K. Li, C. Wang, X. Sun, P. Ning and L. Tang, *Chem. Eng. J.*, 2017, **330**, 727–735.
23 Q. Li, H. Yi, X. Tang, S. Zhao, B. Zhao, D. Liu and F. Gao, *Chem. Eng. J.*, 2016, **284**, 103–111.
24 J. West, B. P. Williams, N. Young, C. Rhodes and G. J. Hutchings, *Catal. Lett.*, 2001, **74**, 111–114.
25 S. C. Lee, Y. M. Kwon, H. J. Chae, S. Y. Jung, J. B. Lee, C. K. Ryu, C. K. Yi and J. C. Kim, *Fuel*, 2013, **104**, 882–885.
26 H. Liu, L. Su, F. Liu, C. Li and U. U. Solomon, *Appl. Catal., B*, 2011, **106**, 550–558.
27 C. Murugan, H. C. Bajaj and R. V. Jasra, *Catal. Lett.*, 2010, **137**, 224–231.
28 S. U. Rege and R. T. Yang, *Chem. Eng. Sci.*, 2001, **56**, 3781–3796.
29 L. Fernández-Carrasco and E. Vázquez, *Fuel*, 2009, **88**, 1533–1538.
30 A. Boumaza, L. Favaro, J. Lédion, G. Sattonnay, J. B. Brubach, P. Berthet, A. M. Huntz, P. Roy and R. Tétot, *J. Solid State Chem.*, 2009, **182**, 1171–1176.
31 K. Li, G. Liu, T. Y. Gao, F. Lu, L. Tang, S. Liu and P. Ning, *Appl. Catal., A*, 2016, **527**, 171–181.
32 M. Liang, C. Li and H. Guo, *J. Fuel Chem. Technol.*, 2002, **30**, 347–352.
33 E. He, G. Huang, H. Fan, C. Yang, H. Wang, Z. Tian, L. Wang and Y. Zhao, *Fuel*, 2019, **246**, 277–284.
34 G. Zhou, Y. Fu and H. Zhou, *Petrochemical Technol.*, 2001, **30**, 602–604.
35 R. Sui, C. B. Lavery, D. Li, C. E. Deering, N. Chou, N. I. Dowling and R. A. Marriott, *Appl. Catal., B*, 2019, **241**, 217–226.
36 Y. Yue, X. Zhao, W. Hua and Z. Gao, *Appl. Catal., B*, 2003, **46**, 561–572.
37 H. Yi, S. Zhao, X. Tang, C. Song, F. Gao, z. Wang, B. Zhang and Y. Zuo, *Catal. Commun.*, 2014, **56**, 106–109.
38 X. Song, P. Ning, C. Wang, K. Li, L. Tang, X. Sun and H. Ruan, *Chem. Eng. J.*, 2017, **314**, 418–433.